Letter Vol. 49, No. 4 / 15 February 2024 / Optics Letters 1093

Optics Letters

Multilayer dielectric reflector using low-index nanolattices

I-TE CHEN, VIJAY ANIRUDH PREMNATH, AND CHIH-HAO CHANG*

Walker Department of Mechanical Engineering, The University of Texas at Austin, Austin, Texas 78712, USA
*chichang@utexas.edu

Received 15 December 2023; revised 29 January 2024; accepted 30 January 2024; posted 31 January 2024; published 15 February 2024

Dielectric mirrors based on Bragg reflection and photonic crystals have broad application in controlling light reflection with low optical losses. One key parameter in the design of these optical multilayers is the refractive index contrast, which controls the reflector performance. This work reports the demonstration of a high-reflectivity multilayer photonic reflector that consists of alternating layers of TiO_2 films and nanolattices with low refractive index. The use of nanolattices enables high-index contrast between the high- and low-index layers, allowing high reflectivity with fewer layers. The broadband reflectance of the nanolattice reflectors with one to three layers has been characterized with peak reflectance of 91.9% at 527 nm and agrees well with theoretical optical models. The high-index contrast induced by the nanolattice layer enables a normalize reflectance band of $\Delta\lambda/\lambda_o$ of 43.6%, the broadest demonstrated to date. The proposed nanolattice reflectors can find applications in nanophotonics, radiative cooling, and thermal insulation.

https://doi.org/10.1364/OL.516147

Introduction. Multilayer dielectric mirrors based on Bragg reflectors and one-dimensional (1D) photonic crystals (PhCs) are attractive over metal-based mirrors and have broad applications in photonics [1–8]. These systems consist of alternating layers of thin films with high and low optical indices, which can be designed by controlling the layer thickness and number. Multilayer reflectors have several key advantages, including that they can be omnidirectional and polarization insensitive within the designed energy bandgap. Based on all dielectric materials, the absorption losses can also be minimized to yield a perfect reflection [8]. Furthermore, the multilayer can be designed and tailored to a specific reflectance band, which can enable wavelength-selective behavior. Such structures have been observed in many species of beetles, which results in the metallic iridescence of their exoskeletons [9,10]. These multilayer reflectors have applications in optoelectronics [2], optical waveguides [6], and passive radiative cooling [10–15].

In these multilayer reflectors, the index contrast is critical and can enhance reflection efficiency and bandwidth [4,6]. Therefore, the use of a low-index material can greatly enhance the performance of these reflectors. Recent work has demonstrated a low-index material with high porosity using the solgel synthesis process with an index as low as 1.1 [16–19]. Glancing angle deposition (GLAD) can also be used to control the porosity of the nanostructured film to yield porous silica with an index down to 1.05. These low-index materials have been adopted to fabricate a multilayer reflector [20–24], and recent work has demonstrated a five-layer reflector with over 99% reflection in the infrared with full width at half maximum (FWHM) of 320 nm with a center wavelength $\lambda_o = 1.33$ µm, yielding $\Delta\lambda/\lambda_o \sim 24.1\%$ [25]. However, the index of the porous Ge used is relatively high, with 1.98 as the low-index layer. More recent work in the visible region using a five-layer stack consisting of low-index porous TiO_2 with $n = 1.438$ has demonstrated $\Delta\lambda = 96$ nm at $\lambda_o = 540$ nm, yielding $\Delta\lambda/\lambda_o = 17.8\%$ [26,27]. Furthermore, most existing low-index materials are based on materials with random porosity, which can have scattering losses and poor mechanical stiffness and strength at low density. One promising alternative is nanolattices [28–30], which have demonstrated a low index down to 1.025 while maintaining high stiffness in the GPa range [31–34]. However, they have not been demonstrated in multilayer PhC reflectors.

This work presents the fabrication and demonstration of a nanolattice multilayer reflector with high reflectivity and broad reflectance band. In this approach low-index nanolattices are integrated into the multilayer PhC reflector and sandwiched between solid high-index films. The nanolattice used has an effective index in the $n = 1.1$ range and allows the index contrast to be significantly increased to enhance the optical response. The reflectance of the fabricated structures with one to three pairs of alternating layers demonstrates high reflectance and a broad reflectance band and agrees with theoretical model based on the transfer matrix method (TMM). The nanolattice reflector has improved performance at reduced number of layers and can find applications in dielectric mirrors, integrated photonics, and multilayer optoelectronic devices.

Technical approach. The normalized wavelength bandwidth of a 1D photonic crystal is proportional to the refractive index contrast between the alternating materials which can be calculated by [6,35]

$$\frac{\Delta\lambda}{\lambda_0} = \frac{4}{\pi}\text{asin}\left(\frac{n_2 - n_1}{n_2 + n_1}\right), \quad (1)$$

where $\Delta\lambda$ is the bandwidth of the stop band, λ_0 is the central wavelength of the bandgap, n_1 and n_2 are the refractive indices of the low- and high-index materials, respectively. In this work, a nanolattice layer (effective $n_1 \approx 1.1$) with 500 nm period and

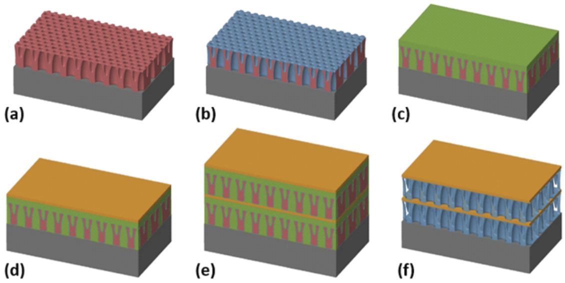

Fig. 1. Fabrication process of the nanolattice reflector. (a) Pattern nanostructures in the photoresist and (b) ALD deposition. (c) Next, the polymer planarization layer is spin coated and (d) the TiO_2 film is deposited. (e) Finally, the process is repeated for the second pair and (f) the polymer template is removed using the thermal cycle.

10 nm Al_2O_3 thickness was deposited using an atomic layer deposition (ALD) and a fully dense TiO_2 film ($n_2 \approx 2.2$) as the low- and high-index materials, respectively. Note that the TiO_2 has a higher index than the bulk Al_2O_3 and is selected to maximize the index mismatch between the reflector and nanolattice layers. The calculated $\Delta\lambda/\lambda_o = 0.46$ is higher than those reported in the literature [20–27]. The transfer matrix method (TMM) is used to simulate the resulting reflection of the dielectric mirror with alternating pairs of low- and high-index materials. In this model the low-index nanolattice layers are assumed to have an isotropic index of 1.1 based on experimental measurements. The TMM model is used to design and model the reflectance spectra for one to three alternating layers of an Al_2O_3 nanolattice with 130 nm height and a TiO_2 film with 80 nm thickness and will be compared with experimental values.

The fabrication process of the nanolattice reflectors is illustrated in Fig. 1. Silicon substrates are initially coated with 100 nm-thick antireflection coating (Brewer Science ARC i-con-16) and photoresist (Sumitomo PFi-88A2). The photoresist is then patterned using colloidal phase lithography with 500 nm diameter nanospheres, as described in prior work [30,36], resulting in nanostructures as shown in Fig. 1(a). The nanostructures are employed as the template for ALD (Cambridge Nano-Tech Inc ALD TM 200), where a conformal Al_2O_3 film with 11.5 nm thickness is coated on the surface, as shown in Fig. 2(b). A thick photoresist layer is then used to planarize the underlying nanolattice, and a continuous TiO_2 film is deposited using electron-beam evaporation (Kurt J. Lesker PVD75), as shown in Figs. 2(c) and 2(d). By repeating the process, multiple nanolattices and TiO_2 layers can be fabricated, as shown in Fig. 2(e). A thermal cycle at 550°C is used to remove the photoresist layers to form a high contrast nanolattice dielectric reflector, as shown in Fig. 2(f). In this process the height of each low-index nanolattice layer can be controlled by the photoresist thickness,

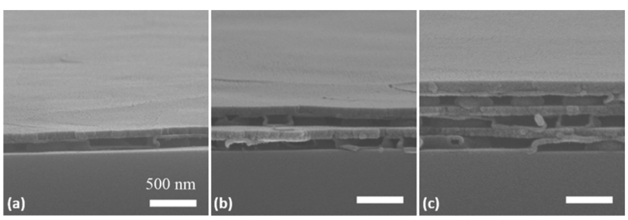

Fig. 2. Cross section SEM images of nanolattices with (a) one, (b) two, and (c) three pairs of 130 nm Al_2O_3 nanolattice and 80 nm TiO_2 layers.

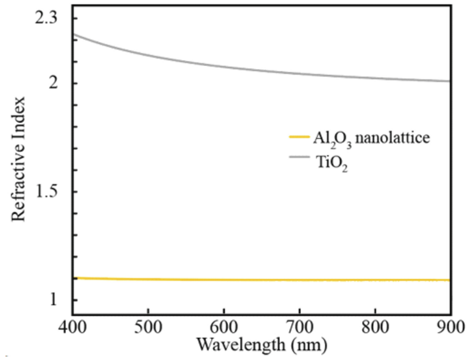

Fig. 3. Measured refraction indices of the nanolattice and TiO_2 layers.

and the thickness of the high-index TiO_2 film is controlled by the evaporation process.

The fabricated nanolattice reflector with one, two, and three pairs of alternating low- and high-index layers is shown in the cross section SEM images in Fig. 2. Here a single pair of the reflector consists of a 130 nm Al_2O_3 nanolattice and an 80 nm TiO_2 film, as shown in Fig. 2(a). Here it can be observed that the nanolattice maintained a uniform height, supporting the TiO_2 film on top. The height of the nanolattice shrinks by about 19.2% during the template removal, therefore a resist thickness of 180 nm is used to obtain the target of 130 nm nanolattice height. The fabricated samples with two and three pairs of the Al_2O_3 nanolattices and TiO_2 layers exhibit the same effects and are shown in Figs. 2(b) and 2(c), respectively. Here it can be observed that the nanolattice layers are able to support the TiO_2 layers to result in free-standing multilayer structures. Some microscale cracks in the TiO_2 films can be observed in the sample, as illustrated in Fig. 2(b). This defect can be attributed to the warping of the brittle film during the template removal. Such effects can be mitigated by reducing the thickness of the TiO_2 film.

Results and discussion. The refractive indices of the Al_2O_3 nanolattices and the TiO_2 layer are examined by ellipsometry, as shown in Fig. 3. Here the nanolattice layer is approximated as a homogeneous, isotropic layer using the Cauchy model on a silicon substrate. Because the nanolattices have porosity over 90%, the refractive index of the nanolattices is close to 1.1. A slight index variation can be observed in the UV around 400 nm due to the material dispersion. The measured refractive index of the 80 nm thick TiO_2 layer on a silicon substrate ranges from 2.0 to 2.2, resulting in an index contrast relative to the nanolattice of up to $\Delta\lambda \sim 1.1$.

The broadband specular reflectance of the fabricated nanolattice reflectors from 400 to 1000 nm under normal incidence is measured by spectrophotometer (Agilent Cary 5000 UV-Vis-NIR) as shown in Fig. 4. The experimental reflectance of the nanolattice reflectors with one, two, and three pairs from 250 to 2500 nm is shown in Fig. 4(a). Here it can be observed that the nanolattice reflectors all show a narrowband with high reflectance in the 500 to 750 nm range. Outside of the stop band the reflectance is around 40%, which is similar to those of the bare silicon. In the long wavelength range outside the designed reflectance band the reflectivity oscillates due to interference effects. Note the measured reflectance has high noise in the range of 800 to 900 nm, which is due to the optics change in the system.

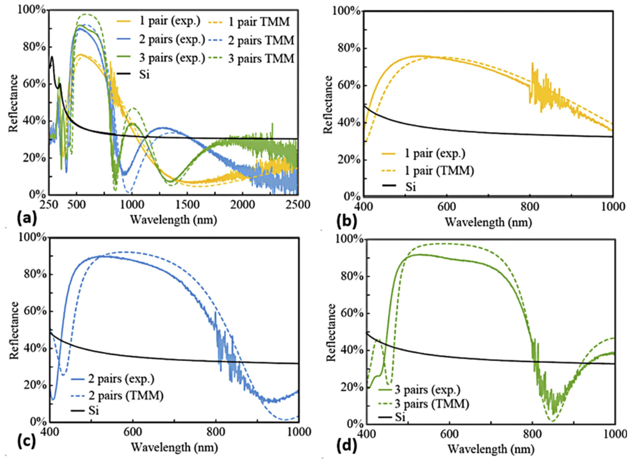

Fig. 4. (a) Broadband specular reflectance fabricated reflectors consisting of a 130 nm tall Al_2O_3 nanolattice and 80 nm thick TiO_2 films at normal incidence. A comparison of the reflectance data and TMM model near the designed reflectance bandwidth for (b) one, (c) two, and (d) three pairs of the alternating films.

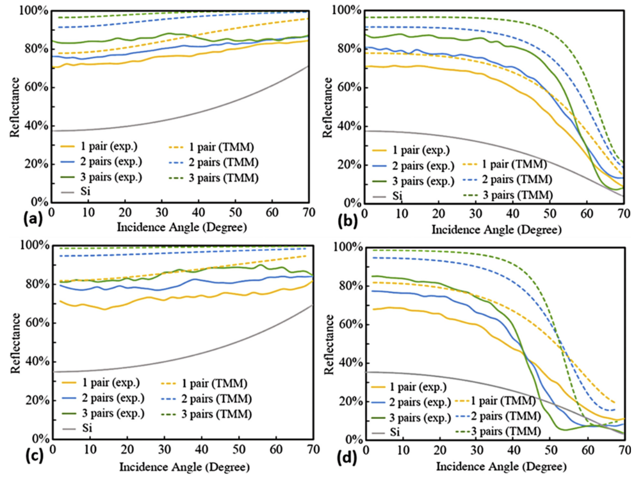

Fig. 5. Specular reflection of the 130 nm Al_2O_3 nanolattice and 80 nm TiO_2 dielectric reflectors as functions of incidence angles. Reflection of (a) TE and (b) TM polarization at 532 nm. Reflection of (c) TE and (d) TM polarization at 633 nm.

A more detailed analysis of the reflectance data for one pair of Al_2O_3 nanolattice and TiO_2 films with TMM model is shown in Fig. 4(b). Here the measured reflectance has a peak value of 75.9% at 538 nm, agreeing well to the predicted peak of 75.2% at 580 nm by the TMM model. Similar trends are observed for the two-pair nanolattice sample where the reflectance has a peak value of 89.9% at 525 nm, and the >80% reflectance band is from 458 to 690 nm, as shown in Fig. 4(c). The data agrees well with the corresponding TMM model, which shows a peak value of 92.1% at 527 nm and the >80% reflectance band from 490 to 730 nm.

The peak reflectance is further improved in the three-pair nanolattice reflector, as shown in Fig. 4(d). Here the measured data has a peak value of 91.9% at 527 nm and the >80% reflection band from 470 to 732 nm. This results in $\Delta\lambda/\lambda_o = 43.6\%$, which is close to the predicted value of 46% from Eq. (1) using $n_1 = 1.1$ and $n_2 = 2.2$. The corresponding TMM model predicts a peak reflectance of 97.8% at 580 nm and the >80% reflectance band from 490 to 750 nm. It can be noted that the measured reflectance for all samples has a slight blueshift to a shorter wavelength, which can be attributed to the nanolattice structures being slightly shorter than the designed height. The peak reflectance is also a bit lower than predicted and is due to fabrication defects and scattering losses.

The specular reflectivity of the fabricated nanolattice reflectors versus the incidence angle is characterized with 633 and 532 nm laser, as shown in Fig. 5. Here the measured reflectance and the corresponding TMM models of the samples with one to three pairs are shown in the solid and dash lines, respectively. The reflectance at 532 nm for the TE polarization is shown in Fig. 5(a). For the sample with one pair, the specular reflectance is around 70.8% at normal incidence and 84.5% at 70°, which agrees well with the TMM model. It can be observed the nanolattice reflector can achieve higher reflectance as the repeating pair number increases from one to three. As the pair number increases to three, the specular reflectance can be as high as 84.5% and 87.2% at 0° and 70° of incidence angles, respectively. Note the measured reflectance is lower than that measured from the spectrophotometer, which can be attributed to sample non-uniformity for the larger laser beam. The increased reflectance versus the number of pairs can also be observed in the TM polarization case, as shown in Fig. 5(b). However, a drop in the reflection can be observed because of the Brewster's angle and that the multilayer stack does not form a complete PhC bandgap. The specular reflectance of the 633 nm wavelength light with TE and TM polarization is shown in Figs. 5(c) and 5(d), respectively, which shows similar angle sensitivity.

It can be noted that the experimental results show that the measured reflectance is lower than the prediction from the TMM simulation. The degradation can be attributed to the defects in the multilayer stack, which results in scattering losses and diffused reflection. Since the nanolattice reflector consists of multiple lithography steps, the defects in each layer would compound and decrease the overall reflectance. The mismatch between the data and the model is more evident at high incidence angle, which is due to the laser beam having a larger projection area, and more defects would be involved in the measurement. The defects in the nanolattices can be mitigated by improving the fabrication yield rate of each layer using more precise lithography techniques, such as interference lithography, which is the subject of on-going work. The thermal treatment cycle can also be further optimized since the structure collapse mostly occurs during the polymer removal process. Future work will focus on demonstrating nanolattice reflectors with additional layers, which is expected to lessen the angle-dependency of the reflectance.

Conclusion. This work demonstrates that nanolattices with low refractive index can be integrated into a multilayer PhC reflector to increase the index contrast and enhance reflectivity. Multilayer reflectors consisting of one to three pairs of 130 nm Al_2O_3 nanolattice and 80 nm TiO_2 layers are fabricated and exhibit high reflectance in the designed stop band. The nanolattice reflector with three pairs has demonstrated peak reflectance of 91.9% with >80% reflectance over a bandwidth of 470 to 732 nm, which is achieved using only three alternating layers. The reflector results in $\Delta\lambda/\lambda_o = 43.6\%$, which is close to the predicted values given the high-index contrast of $\Delta n \sim 1$. The resulting nanolattice reflectors can be designed to have a reflectance band by controlling the thicknesses of the nanolattice and TiO_2 layers. This work demonstrates the potential of integrating nanolattices in multilayer reflectors and can find applications in nanophotonics, optoelectronics, and radiative cooling.

Funding. Directorate for Technology, Innovation and Partnerships (TI-2314268); Energy Institute at the University of Texas at Austin.

Acknowledgment. This work was performed at UT Austin Texas Materials Institute (TMI), the Nanomanufacturing System for mobile Computing and Energy Technologies (NASCENT), and Texas Nanofabrication Facilities, which is supported by the National Science Foundation (NSF) as part of the National Nanotechnology Coordinated Infrastructure (NNCI) grant NNCI-2025227.

Disclosures. The authors declare no conflict of interest.

Data availability. No additional data were generated or analyzed in the presented research.

REFERENCES

1. A. Yariv and P. Yeh, *Optical Waves in Crystals*, Wiley Series in Pure and Applied Optics (Wiley, 1984).
2. S. Wang, IEEE J. Quantum Electron. **10**, 413 (1974).
3. J. Lekner, J. Opt. Soc. Am. A **11**, 2892 (1994).
4. C. J. R. Sheppard, Pure Appl. Opt. **4**, 665 (1995).
5. J. N. Winn, Y. Fink, S. Fan, *et al.*, Opt. Lett. **23**, 1573 (1998).
6. Y. Fink, J. N. Winn, S. Fan, *et al.*, Science **282**, 1679 (1998).
7. D. N. Chigrin, A. V. Lavrinenko, D. A. Yarotsky, *et al.*, Appl. Phys. A: Mater. Sci. Process. **68**, 25 (1999).
8. G.-W. Truong, L. W. Perner, D. M. Bailey, *et al.*, Nat. Commun. **14**, 7846 (2023).
9. A. E. Seago, P. Brady, J.-P. Vigneron, *et al.*, J. R. Soc. Interface. **6**, S165 (2009).
10. S. R. Mouchet and O. Deparis, *Natural Photonics and Bioinspiration* (Artech House Publisher, 2021).
11. A. P. Raman, M. A. Anoma, L. Zhu, *et al.*, Nature **515**, 540 (2014).
12. X. Lim, Nature **577**, 18 (2020).
13. N. W. Pech-May and M. Retsch, Nanoscale Adv. **2**, 249 (2020).
14. S. Liu, C. Sui, M. Harbinson, *et al.*, Nano Lett. **23**, 7767 (2023).
15. A. R. Gentle and G. B. Smith, Adv. Sci. **2**, 1500119 (2015).
16. D. B. Mahadik, R. V. Lakshmi, and H. C. Barshilia, Sol. Energy Mater. Sol. Cells **140**, 61 (2015).
17. B. Wang, C. J. Ruud, J. S. Price, *et al.*, Nano Lett. **19**, 787 (2019).
18. C. J. Ruud, A. Cleri, J.-P. Maria, *et al.*, Nano Lett. **22**, 7358 (2022).
19. R. Danz, B. Elling, A. Buchtemann, *et al.*, IEEE Trans. Dielectr. Electr. Insul. **11**, 286 (2004).
20. J. Lekner, J. Opt. A: Pure Appl. Opt. **2**, 349 (2000).
21. J.-Q. Xi, M. Ojha, W. Cho, *et al.*, Opt. Lett. **30**, 1518 (2005).
22. M. F. Schubert, J.-Q. Xi, J. K. Kim, *et al.*, Appl. Phys. Lett. **90**, 141115 (2007).
23. M. N. Ghazzal, O. Deparis, J. De Coninck, *et al.*, J. Mater. Chem. C **1**, 6202 (2013).
24. S. Guldin, M. Kolle, M. Stefik, *et al.*, Adv. Mater. **23**, 3664 (2011).
25. J. W. Leem and J. S. Yu, Opt. Express **20**, 20576 (2012).
26. S. H. Lee, J. W. Leem, X.-Y. Guan, *et al.*, Thin Solid Films **591**, 351 (2015).
27. J. W. Leem, X.-Y. Guan, and J. S. Yu, Opt. Express **22**, 18519 (2014).
28. T. A. Schaedler, A. J. Jacobsen, A. Torrents, *et al.*, Science **334**, 962 (2011).
29. L. R. Meza, S. Das, and J. R. Greer, Science **345**, 1322 (2014).
30. X. Zheng, H. Lee, T. H. Weisgraber, *et al.*, Science **344**, 1373 (2014).
31. X. A. Zhang, A. Bagal, E. C. Dandley, *et al.*, Adv. Funct. Mater. **25**, 6644 (2015).
32. A. Bagal, X. A. Zhang, R. Shahrin, *et al.*, Sci. Rep. **7**, 9145 (2017).
33. I. Chen, Z. Dai, D. T. Lee, *et al.*, Adv. Mater. Interfaces **8**, 2100690 (2021).
34. V. A. Premnath and C.-H. Chang, Opt. Lett. **48**, 6356 (2023).
35. B. Osting, Appl. Math. Lett. **25**, 1926 (2012).
36. C.-H. Chang, L. Tian, W. R. Hesse, *et al.*, Nano Lett. **11**, 2533 (2011).